

## Research Article

# Galactic Halo Wormhole Solutions in $f(T)$ Gravity

M. Sharif<sup>1</sup> and Shamaila Rani<sup>1,2</sup>

<sup>1</sup> Department of Mathematics, University of the Punjab, Quaid-e-Azam Campus, Lahore 54590, Pakistan

<sup>2</sup> Department of Mathematics, University of Management and Technology, Johar Town Campus, Lahore 54782, Pakistan

Correspondence should be addressed to M. Sharif; msharif.math@pu.edu.pk

Received 23 July 2014; Accepted 14 November 2014; Published 27 November 2014

Academic Editor: Shi-Hai Dong

Copyright © 2014 M. Sharif and S. Rani. This is an open access article distributed under the Creative Commons Attribution License, which permits unrestricted use, distribution, and reproduction in any medium, provided the original work is properly cited. The publication of this article was funded by SCOAP<sup>3</sup>.

The proposal of galactic halo region is based on the idea that dark halos contain some characteristics needed to support traversable wormhole solutions. We explore wormhole solutions in this region in the framework of generalized teleparallel gravity. We consider static spherically symmetric wormhole spacetime with flat galactic rotational curves and obtain expressions of matter components for nondiagonal tetrad. The effective energy-momentum tensor leads to the violation of energy conditions which may impose condition on the normal matter to satisfy these conditions. We take two well-known  $f(T)$  models in exponential and logarithmic forms to discuss wormhole solutions as well as the equilibrium condition. It is concluded that wormhole solutions violating weak energy condition are obtained for both models with stable configuration.

## 1. Introduction

It is a well-known fact that dark matter (DM) constituents in the universe exist in baryonic and nonbaryonic forms. Astronomers can easily detect some types of DM through the emission of photons in all directions which emit light. This type of matter is in the terms of baryonic DM which is less than 4% of the overall density of the universe. It is argued that the remaining baryonic DM is in the nonluminous form such as MACHOs which may fulfill the required percentage of baryonic matter in the universe. However, the second major constituent of the universe is nonbaryonic DM and its contribution is approximately 23%. This matter cannot be detected directly because it does not absorb, emit, or scatter light of any wavelength.

The presence of DM in halo is deduced from its gravitational impression on rotational curves of a spiral galaxy [1–3]. The standard model could not explain this phenomenon of flat rotational curves observed in the galaxies. In particular, the baryonic DM fails to give any clue about these rotational curves related to neutral hydrogen clouds even located in the outer region of galaxies. This leads to the hypothesis that the nonluminous matter, that is, DM, is taken as the cause for the rotational curves. However, its presence can be

detected only through its gravitational influence on visible DM. The main possible candidates of nonbaryonic matter are weakly interacting massive particles [4], supersymmetry [5], modified theories [6, 7], and scalar fields [8, 9].

Navarro et al. [10, 11] discussed the structure of dark halos by taking N-body numerical simulations and found the density profile of these halos in the standard model of cosmology. This scenario leads to the energy density of galactic halo regions (galaxies and cluster of galaxies) as

$$\rho_s = \frac{r_s K}{r} \left( 1 + \frac{r}{r_s} \right)^{-2}, \quad (1)$$

where  $r_s$  represents characteristics scale radius and  $K$  is the corresponding density. This equation is referred to as Navarro-Frenk-White density profile. It has been proved that the geometry of dark galactic halo may be distinguished by the traversable wormhole spacetime along with density profile as well as flat galactic rotational curves. Rahaman et al. [12] argued that these galactic halo regions possess some characteristics to support the wormhole solution. They found the equilibrium condition for this solution and detected it through scattered scalar waves. Kuhfittig [13] discussed the

gravitational lensing of wormhole solution in the galactic halo region.

A wormhole is a hypothetical path to connect different regions of the universe. This path can be regarded as a tunnel or bridge from which the observer may traverse easily. In general relativity, the exotic matter (which violates the energy conditions) constitutes basic ingredient to develop mathematical structure of wormhole. The violation of null energy condition is the necessary tool to form wormhole solutions which also allow two-way travel. The search for a realistic source which provides this violation (while normal matter may satisfy the energy conditions) has gained a lot of interest nowadays. This search introduced modified theories of gravity, dynamical spacetime, scalar field, non-commutative geometry, electromagnetic field, and so forth in wormhole scenario. In modified theories of gravity, the effective energy-momentum tensor is responsible for the corresponding violation while normal matter threads wormhole solutions.

The  $f(T)$  theory of gravity (generalized teleparallel theory) has attracted many people to explore it in different physical scenarios like accelerated expansion of the universe [14, 15], solar system tests [16], charged black hole solutions [17], Noether symmetry [18], wormhole solutions [19, 20], thermodynamics [21, 22], and many more. Böhmer et al. [20] were the first who studied wormhole solutions in this gravity by taking static spherically symmetric traversable wormhole solutions and found some constraints on the wormhole throat. The behavior of energy conditions is explored by taking particular shape as well as redshift functions. The power-law form of  $f(T)$  model, which is the sum of linear and quadratic terms, is considered and physically acceptable solutions are obtained. Jamil et al. [23] studied these solutions by taking fluid as isotropic and anisotropic as well as particular equation of state. They assumed a viable power-law  $f(T)$  model which consists of teleparallel and square-root terms in order to compare the results with general relativity. They found that energy conditions are violated in anisotropic case while these are satisfied for the remaining two cases. We explored dynamical wormhole solutions for traceless as well as barotropic equations of state [24] using analytic and numerical  $f(T)$  models and concluded that weak energy condition (WEC) holds in specific time intervals for these cases.

Recently, we have studied wormhole solutions [25] in the background of noncommutative geometry for  $f(T) = \alpha T^n$  model as well as shape function. It was found that the effective energy-momentum tensor serves as the basic ingredient to thread the wormhole solutions and normal matter gives some physically acceptable solutions. Here we extend [26] this work to study the effects of electrostatic field. In this paper, we explore static spherically symmetric wormhole solutions in the galactic halo region. We consider exponential as well as logarithmic  $f(T)$  models and study the shape function to set up wormhole scenario as well as to check the behavior of WEC. The paper is organized as follows. The next section provides overview of  $f(T)$  field equations and energy conditions. In Section 3, we construct matter components for wormhole solutions in the galactic

halo region. Section 4 is devoted to the exploration of these solutions for two well-known  $f(T)$  models. Also, we check the equilibrium conditions of both solutions. The last section summarizes the results.

## 2. $f(T)$ Gravity and Energy Conditions

In this section, we briefly overview  $f(T)$  gravity and energy conditions. The action for the generalized teleparallel gravity is defined as [27–30]

$$\mathcal{S} = \frac{1}{16\pi\mathcal{E}} \int d^4x h (f(T) + \mathcal{L}_m), \quad (2)$$

where  $h = \det(h_\mu^i)$ ,  $h_\mu^i$  denotes the tetrad,  $\mathcal{L}_m$  is the matter Lagrangian, and  $f$  is an arbitrary differentiable function of the torsion scalar  $T$ . The tetrad field is an orthonormal set of four-vector fields which is the basic entity in developing the torsion tensor as well as torsion scalar for this gravity. The tetrad variation of this action yields the following field equations:

$$\left[ \frac{1}{h} \partial_\mu (h h_\nu^\lambda S_\lambda^{\mu\nu}) + h_\nu^\lambda T_{\mu\gamma}^\lambda S_\lambda^{\mu\nu} \right] f_T + h_\nu^\lambda S_\lambda^{\mu\nu} \partial_\mu (T) f_{TT} + \frac{1}{4} h_\nu^\lambda f = \frac{1}{2} \kappa^2 h_\nu^\lambda \mathcal{T}_\nu^\lambda, \quad (3)$$

where  $f_T = df/dT$ ,  $f_{TT} = d^2f/dT^2$ , and  $\mathcal{T}_\nu^\lambda$  is the matter tensor. The torsion scalar is defined as

$$T = T_{\mu\nu}^\lambda S_\lambda^{\mu\nu}. \quad (4)$$

Here the antisymmetric torsion and superpotential tensors are

$$T_{\mu\nu}^\lambda = h_\nu^i (\partial_\nu h_\mu^i - \partial_\mu h_\nu^i), \quad (5)$$

$$S_\nu^{\mu\gamma} = \frac{1}{2} (K_\nu^{\mu\gamma} + \delta_\nu^\mu T_\alpha^{\alpha\gamma} - \delta_\nu^\gamma T_\alpha^{\alpha\mu}),$$

and  $K_\nu^{\mu\gamma}$  is the contorsion tensor given by

$$K_\nu^{\mu\gamma} = -\frac{1}{2} (T_\nu^{\mu\gamma} - T_\nu^{\gamma\mu} - T_\nu^{\mu\gamma}). \quad (6)$$

The covariant reconstruction of the field equations provides equivalence between Einstein-Hilbert and generalized teleparallel gravity actions. Rearranging all the partial derivatives in (5) and (6), replacing them by covariant derivatives, and using the compatibility of the metric tensor,  $\nabla_\sigma g_{\mu\nu} = 0$ , the relations  $S^{\mu(\nu\gamma)} = T^{\mu(\nu\gamma)} = K^{(\mu\nu)\gamma} = 0$  with  $S_{\rho\mu}^\mu = -2T_{\rho\mu}^\mu = 2K_{\rho\mu}^\mu$  lead to  $R+T = -2\nabla^\mu T_{\mu\nu}^\nu$ . This implies that  $T$  and  $R$  differ only by covariant divergence of the torsion tensor. Using these relations with Einstein tensor,  $G_{\mu\nu} = R_{\mu\nu} - (1/2)g_{\mu\nu}R$ , we obtain after some manipulations

$$G_{\mu\nu} - \frac{1}{2}g_{\mu\nu}T = -S_{\mu}^{\rho\sigma} K_{\sigma\rho\nu} - \nabla^\sigma S_{\nu\sigma\mu}. \quad (7)$$

Substituting this equation in (3), the field equations become

$$f_T G_{\mu\nu} + D_{\mu\nu} f_{TT} + \frac{1}{2} g_{\mu\nu} (f - T f_T) = \kappa^2 \mathcal{T}_{\mu\nu}, \quad (8)$$

where  $D_{\mu\nu} = S_{\nu\mu}^\gamma \nabla_\gamma T$ . The trace equation takes the form

$$Df_{TT} - (R + 2T) f_T + 2f = \kappa^2 \mathcal{T}, \quad (9)$$

with  $D = D_\rho^\rho$  and  $\mathcal{T} = \mathcal{T}_\rho^\rho$ . The  $f(T)$  field equations can be rewritten as

$$G_{\mu\nu} = \frac{\kappa^2}{f_T} (\mathcal{T}_{\mu\nu} + \widetilde{\mathcal{T}}_{\mu\nu}), \quad (10)$$

where torsion contribution through trace equation yields

$$\widetilde{\mathcal{T}}_{\mu\nu} = \frac{1}{\kappa^2} \left[ -D_{\mu\nu} f_{TT} - \frac{1}{4} g_{\mu\nu} (\mathcal{T} - Df_{TT} + Rf_T) \right]. \quad (11)$$

The energy conditions are used to work out many general results in different physical scenarios. The violation of these conditions in general relativity leads to the construction of wormhole solutions. The Raychaudhuri equation and attractiveness of gravity yield the energy conditions as

- (i)  $\rho + p \geq 0$ ,
- (ii)  $\rho + p \geq 0$ ,  $\rho + 3p \geq 0$ ,
- (iii)  $\rho \geq 0$ ,  $\rho \pm p \geq 0$ ,
- (iv)  $\rho \geq 0$ ,  $\rho + p \geq 0$ ,

null, strong, dominant, and weak energy conditions, respectively. Here,  $\rho$  and  $p$  represent the energy density and pressure of perfect fluid. In modified theories of gravity, these conditions are modified in terms of effective energy density and pressure; for example, WEC becomes  $\rho_{\text{eff}} \geq 0$ ,  $\rho_{\text{eff}} + p_{\text{eff}} \geq 0$ . We discuss the behavior of WEC in order to explore wormhole solutions in the galactic halo region.

### 3. Wormhole Geometry in the Galactic Halo Region

Here, we provide wormhole scenario in the galactic halo region and construct matter contributions using effective formalism. The static spherically symmetric spacetime representing wormhole geometry is given by

$$ds^2 = e^{2g(r)} dt^2 - \left(1 - \frac{s(r)}{r}\right)^{-1} dr^2 - r^2 (d\theta^2 + \sin^2\theta d\phi^2), \quad (12)$$

where  $g(r)$  denotes redshift function which corresponds to gravitational redshift and  $s(r)$  is the shape function which determines shape of the wormhole. The redshift must satisfy the no-horizon condition which allows two-way travel implying that  $g(r)$  must be finite everywhere in the spacetime. This shape function satisfies flaring-out conditions which depend on the radius of wormhole throat, the minimum value of  $r$ . To discuss wormhole geometry, it is very important to locate the throat so that traversability of the wormhole solution is guaranteed. The flaring-out conditions constitute  $(s - s'r)/r^2 > 0$  for the throat radius  $r_0$  and  $s(r) = r_0$  at  $r = r_0$  along with  $s'(r_0) < 1$ . At large distances, the spacetime should meet the asymptotically flat condition; that is,  $s(r)/r \rightarrow 0$  as

$r \rightarrow \infty$ . The condition  $1 - s/r > 0$  also requires to be met at throat. A suitable form for the redshift function obtained from flat rotational curve is given by [1–3, 12, 13]

$$e^{2g(r)} = cr^m, \quad (13)$$

where  $m = 2(v^\phi)^2$ ,  $v^\phi$  is the rotational velocity in the DM region which is nearly constant through rotational curve profile. Also,  $c$  is an integration constant taken as  $c = (1/r_s)^m$  for the sake of simplicity. We assume anisotropic matter distribution for which the energy-momentum tensor is

$$\mathcal{T}_\beta^\alpha = (\rho + p_t) U^\alpha U_\beta - p_t \delta_\beta^\alpha + (p_r - p_t) V^\alpha V_\beta, \quad (14)$$

where  $p_r$  and  $p_t$  are the radial and transverse components of pressure. The four velocity of the fluid  $U^\alpha$  and the unit spacelike vector  $V^\alpha$  satisfy  $U^\alpha U_\alpha = 1$ ,  $V^\alpha V_\alpha = -1$ , and  $U^\alpha V_\alpha = 0$ . The corresponding energy-momentum tensor is

$$\mathcal{T}_\beta^\alpha = \text{diag}(\rho(r), -p_r(r), -p_t(r), -p_t(r)). \quad (15)$$

For static spherically symmetric spacetime, the diagonal tetrad leads  $f(T)$  gravity to teleparallel gravity. In order to find out wormhole solutions, we consider nondiagonal tetrad representing the most favorable choice for  $f(T)$  gravity. The tetrad components for the metric (12) are given by

$$h_\mu^i = \begin{pmatrix} \left(\frac{r}{r_s}\right)^{m/2} & 0 & 0 & 0 \\ 0 & \frac{1}{\sqrt{1-(s/r)}} \sin\theta \cos\phi & r \cos\theta \cos\phi & -r \sin\theta \sin\phi \\ 0 & \frac{1}{\sqrt{1-(s/r)}} \sin\theta \sin\phi & r \cos\theta \sin\phi & r \sin\theta \cos\phi \\ 0 & \frac{1}{\sqrt{1-(s/r)}} \cos\theta & -r \sin\theta & 0 \end{pmatrix}, \quad (16)$$

where  $s = s(r)$ . The torsion scalar turns out as

$$T = \frac{2}{r^2} \left[ 2 \left(1 - \sqrt{1 - \frac{s}{r}}\right) - \frac{s}{r} + m \left(1 - \frac{s}{r} - \sqrt{1 - \frac{s}{r}}\right) \right]. \quad (17)$$

Equation (10) yields the following field equations:

$$\begin{aligned} \frac{\rho}{f_T} - \frac{1}{r} \left(1 - \frac{s}{r} - \sqrt{1 - \frac{s}{r}}\right) T' \frac{f_{TT}}{f_T} - \frac{J}{f_T} &= \frac{s'}{r^2}, \\ \frac{p_r}{f_T} + \frac{J}{f_T} &= \frac{1}{r^2} \left(m \left(1 - \frac{s}{r}\right) - \frac{s}{r}\right), \\ \frac{p_t}{f_T} - \frac{1}{2r} \left(\sqrt{1 - \frac{s}{r}} - \left(1 + \frac{m}{2}\right) \left(1 - \frac{s}{r}\right)\right) T' \frac{f_{TT}}{f_T} + \frac{J}{f_T} \\ &= \frac{1}{2r^2} \left[\frac{m^2}{2} \left(1 - \frac{s}{r}\right) - \left(1 + \frac{m}{2}\right) \left(s' - \frac{s}{r}\right)\right], \end{aligned} \quad (18)$$

where prime refers to derivative with respect to  $r$  and  $J(r)$  is given by

$$J(r) = \frac{1}{4} (\mathcal{T} - Df_{TT} + Rf_T). \quad (19)$$

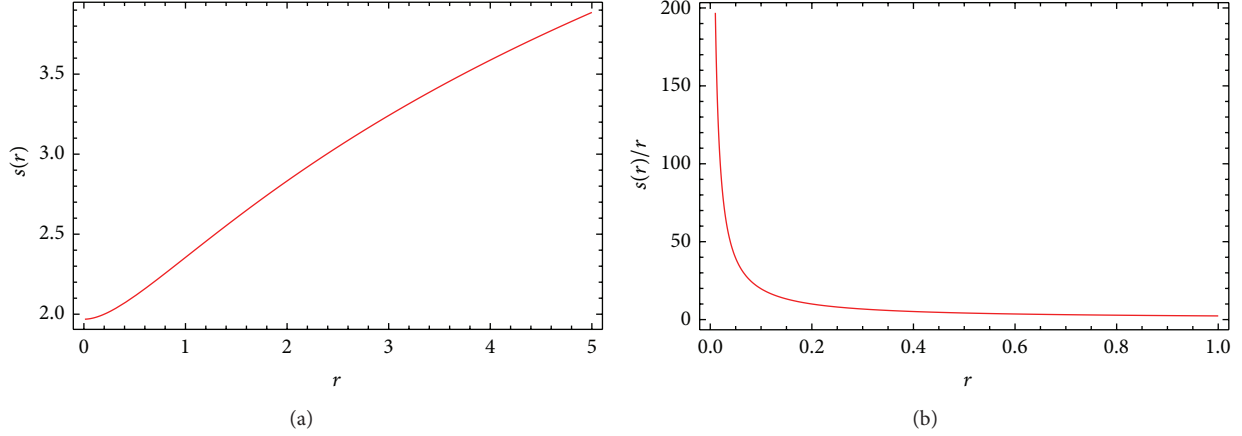


FIGURE 1: Plots of  $s(r)$  (a) and  $s(r)/r$  (b) versus  $r$  for exponential model.

Finally, the field equations (18) can be written as

$$\rho = \frac{s'}{r^2} f_T + \frac{1}{r} \left( 1 - \frac{s}{r} - \sqrt{1 - \frac{s}{r}} \right) T' f_{TT}, \quad (20)$$

$$p_r = \frac{1}{r^2} \left( m \left( 1 - \frac{s}{r} \right) - \frac{s}{r} \right) f_T, \quad (21)$$

$$p_t = \frac{1}{2r} \left( \sqrt{1 - \frac{s}{r}} - \left( 1 + \frac{m}{2} \right) \left( 1 - \frac{s}{r} \right) \right) T' f_{TT} + \frac{1}{2r^2} \left[ \frac{m^2}{2} \left( 1 - \frac{s}{r} \right) - \left( 1 + \frac{m}{2} \right) \left( s' - \frac{s}{r} \right) \right] f_T. \quad (22)$$

Using  $\rho = \rho_s$  in (20) and inserting the value of  $\rho_s$  from (1), we obtain

$$s' f_T + r \left( 1 - \frac{s}{r} - \sqrt{1 - \frac{s}{r}} \right) T' f_{TT} = \frac{K r r_s}{(1 + (r/r_s))^2}, \quad (23)$$

which involves two unknowns,  $s(r)$  and  $f(T)$ . For the wormhole structure and WEC, we have to choose one of these functions. It has been proved in effective scenario that the effective energy-momentum tensor indicates the existence of wormhole solutions. Here, it satisfies when the following inequality holds:  $\rho^{\text{eff}} + p_r^{\text{eff}} = ((s' r - s)/r^3) + (2m/r^2)(1 - (s/r)) < 0$ .

#### 4. Wormhole Solutions for Specific $f(T)$ Models

In this section, we explore wormhole solutions by taking two specific viable models, exponential and logarithmic  $f(T)$  models. We also construct equilibrium conditions for these solutions.

**4.1. Exponential Model.** Firstly, we consider model in exponential form as [31]

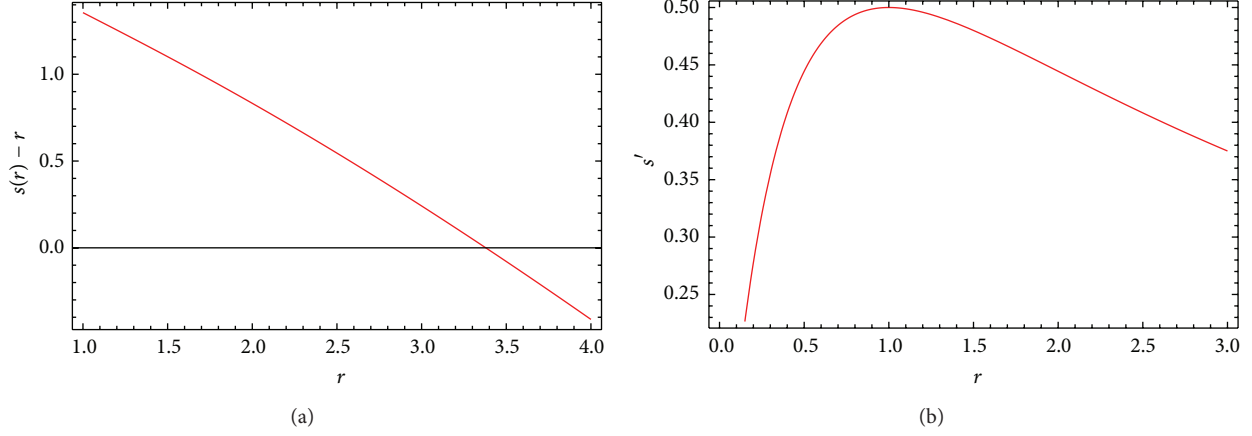
$$f(T) = T - \alpha T \left( 1 - e^{\beta T_0/T} \right), \quad (24)$$

where  $\alpha$ ,  $\beta$  are constants and  $T_0$  represents current value of the torsion scalar. This model undergoes some cosmological

viability conditions; for example, it behaves like  $\Lambda$ CDM for the limit  $\beta = 0$ . For  $T \rightarrow \infty$ , this model satisfies the condition  $f/T \rightarrow 1$  at higher values of redshift consistent with observational constraints from the primordial nucleosynthesis and cosmic microwave background. The redshift function given in (13) takes the form  $g(r) = m/r$ . Inserting this model in (23), it follows that

$$\begin{aligned} & s' \left[ 1 - \alpha + \alpha \left( 1 - \frac{\beta T_0}{T} \right) e^{\beta T_0/T} \right] - \frac{2}{r^2} \left( 1 - \frac{s}{r} - \sqrt{1 - \frac{s}{r}} \right) \\ & \times \left[ -\frac{2s}{r} + 4 \left( 1 - \sqrt{1 - \frac{s}{r}} \right) \right. \\ & \quad \left. + \frac{r s' - s}{r} \left( 1 - \frac{1}{\sqrt{1 - (s/r)}} \right) \right. \\ & \quad \left. + \left\{ 2 \left( 1 - \sqrt{1 - \frac{s}{r}} \right) - \frac{2s}{r} \right. \right. \\ & \quad \left. \left. + \frac{r s' - s}{r} \left( 1 - \frac{1}{2\sqrt{1 - (s/r)}} \right) \right\} \right. \\ & \quad \left. \times \frac{T_0^2}{T^3} m \alpha \beta^2 e^{\beta T_0/T} \right] \\ & = \frac{K r r_s}{(1 + (r/r_s))^2}. \end{aligned} \quad (25)$$

We check the behavior of shape function and flaring-out conditions numerically through graphs by taking arbitrary values of the parameters such as  $\alpha = -0.04$ ,  $\beta = 0.0000002$ ,  $m = 0.02$ ,  $K = 2$ ,  $r_s = 1$ , and  $T_0 = -0.2$ . Figure 1(a) represents the increasing behavior of shape function versus  $r$ . In Figure 1(b),  $s/r$  versus  $r$  is plotted to check the asymptotically flat condition. This shows that  $s/r$  approaches to zero as we increase  $r$  which represents that flatness is asymptotically obtained. To locate the throat of the wormhole, we plot  $s(r) - r$  versus  $r$  as shown in the plot of Figure 2(a). The throat of

FIGURE 2: Plots of  $s(r) - r$  (a) and  $s'$  (b) versus  $r$  for exponential model.

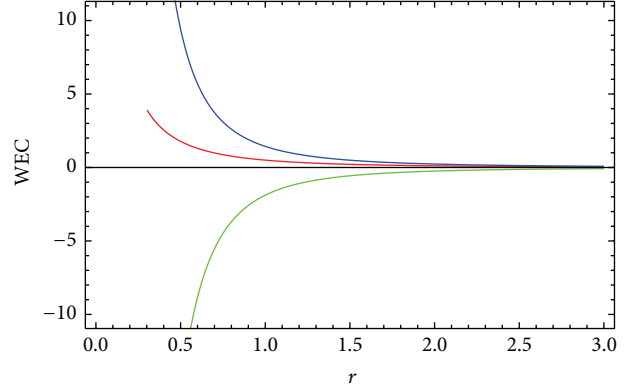
the wormhole is that value of  $r$  at which  $s(r) - r$  crosses or meets the  $r$ -axis. In this plot, the throat is located at  $r = 3.374$ ; that is,  $r_0 = 3.374$ . The first derivative of shape function,  $s'$ , is also plotted versus  $r$  as shown in Figure 2(b), which indicates that  $s'$  at  $r_0$  satisfies the condition  $s'(r_0) < 1$  as  $s'(3.374) = 0.3527 < 1$ . Also, the condition  $s(r_0) = r_0$  is satisfied as shown in Figure 1(a).

To check the behavior of WEC for exponential model, the expressions of matter content using (20)–(22) are given by

$$\begin{aligned} \rho = & \frac{s'}{r^2} \left[ 1 - \alpha + \alpha \left( 1 - \frac{\beta T_0}{T} \right) e^{\beta T_0/T} \right] \\ & - \frac{2}{r^4} \left( 1 - \frac{s}{r} - \sqrt{1 - \frac{s}{r}} \right) \\ & \times \left[ -\frac{2s}{r} + 4 \left( 1 - \sqrt{1 - \frac{s}{r}} \right) + \frac{rs' - s}{r} \right. \\ & \times \left( 1 - \frac{1}{\sqrt{1 - (s/r)}} \right) \\ & \left. + \left\{ 2 \left( 1 - \sqrt{1 - \frac{s}{r}} \right) - \frac{2s}{r} \right. \right. \\ & \left. \left. + \frac{rs' - s}{r} \left( 1 - \frac{1}{2\sqrt{1 - (s/r)}} \right) \right\} \right. \\ & \left. \times \frac{T_0^2}{T^3} m \alpha \beta^2 e^{\beta T_0/T} \right], \end{aligned} \quad (26)$$

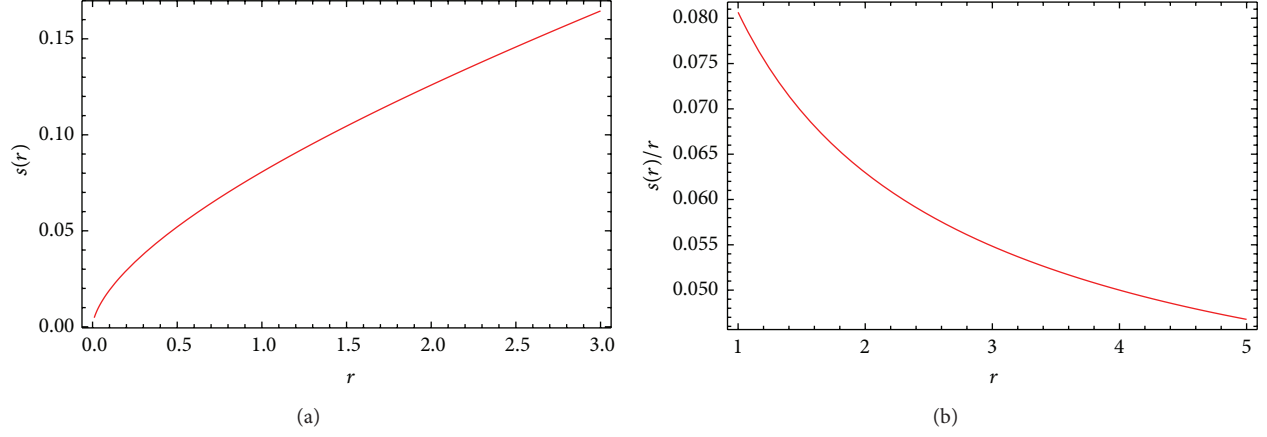
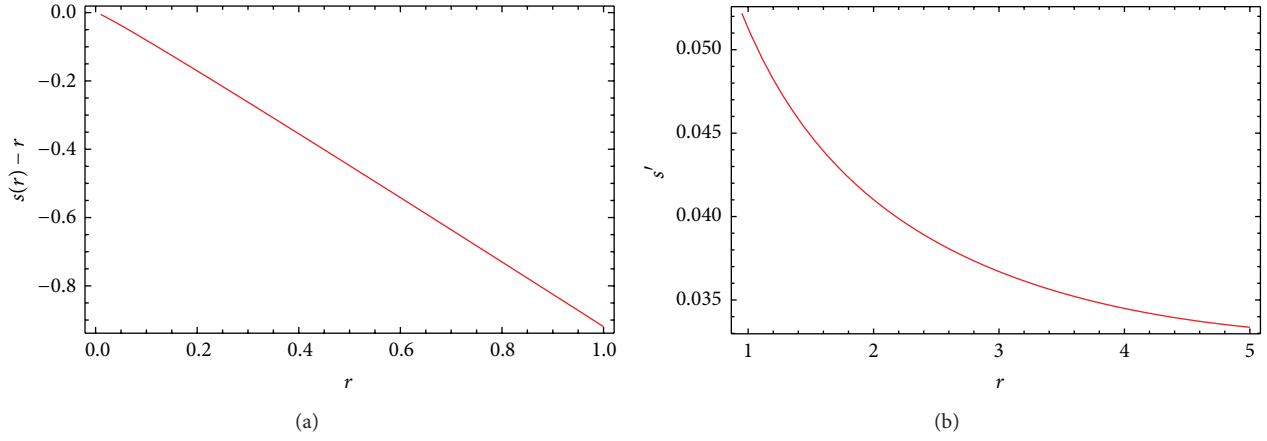
$$P_r = \frac{1}{r^2} \left\{ m \left( 1 - \frac{s}{r} \right) - \frac{s}{r} \right\} \left[ 1 - \alpha + \alpha \left( 1 - \frac{\beta T_0}{T} \right) e^{\beta T_0/T} \right], \quad (27)$$

$$\begin{aligned} P_t = & \frac{1}{2r^2} \left( 1 - \alpha + \alpha \left( 1 - \frac{\beta T_0}{T} \right) e^{\beta T_0/T} \right) \\ & \times \left[ \frac{m^2}{2} \left( 1 - \frac{s}{r} \right) - \left( 1 + \frac{m}{2} \right) \times \left( s' - \frac{s}{r} \right) \right] \end{aligned}$$

FIGURE 3: Plots of WEC:  $\rho$  versus  $r$  (red curve),  $\rho + p_r$  versus  $r$  (green curve), and  $\rho + p_t$  (blue curve) versus  $r$  for exponential model.

$$\begin{aligned} & - \frac{1}{r^4} \left( \sqrt{1 - \frac{s}{r}} - \left( 1 + \frac{m}{2} \right) \left( 1 - \frac{s}{r} \right) \right) \\ & \times \left[ -\frac{2s}{r} + 4 \left( 1 - \sqrt{1 - \frac{s}{r}} \right) + \frac{rs' - s}{r} \right. \\ & \times \left( 1 - \frac{1}{\sqrt{1 - (s/r)}} \right) \\ & \left. + \left\{ 2 \left( 1 - \sqrt{1 - \frac{s}{r}} \right) - \frac{2s}{r} + \frac{rs' - s}{r} \right. \right. \\ & \left. \left. \times \left( 1 - \frac{1}{2\sqrt{1 - (s/r)}} \right) \right\} \frac{T_0^2}{T^3} m \alpha \beta^2 e^{\beta T_0/T} \right]. \end{aligned} \quad (28)$$

Figure 3 represents the graph of these expressions versus  $r$  which indicate that  $\rho$  and  $\rho + p_t$  show decreasing behavior but remain positive while behavior of  $\rho + p_r$  is negative. Thus, the WEC is violated for wormhole solution in the galactic halo region.

FIGURE 4: Plots of  $s(r)$  (a) and  $s(r)/r$  (b) versus  $r$  for logarithmic model.FIGURE 5: Plots of  $s(r) - r$  (a) and  $s'$  (b) versus  $r$  for logarithmic model.

4.2. *Logarithmic Model.* Here we assume model in logarithmic form as [32]

$$f(T) = \gamma T_0 \left( \frac{T}{qT_0} \right)^{1/2} \ln \left( \frac{qT_0}{T} \right), \quad (29)$$

where  $\gamma$  and  $q$  are arbitrary constants. This model represents cosmological viability by showing accelerated expansion of the universe. Substituting this model in (23), we obtain the following differential equation in terms of shape function:

$$\begin{aligned} s' & \left[ \frac{\gamma}{2q} \left( \frac{qT_0}{T} \right)^{1/2} \ln \left( \frac{qT_0}{T} \right) - \frac{\gamma T_0}{T} \left( \frac{T}{qT_0} \right)^{1/2} \right] \\ & - \frac{2}{r^2} \left( 1 - \frac{s}{r} - \sqrt{1 - \frac{s}{r}} \right) \\ & \times \left[ -\frac{2s}{r} + 4 \left( 1 - \sqrt{1 - \frac{s}{r}} \right) \right. \\ & \left. + \frac{rs' - s}{r} \left( 1 - \frac{1}{\sqrt{1 - (s/r)}} \right) \right] \end{aligned}$$

$$\begin{aligned} & + m \left\{ -\frac{2s}{r} + 2 \left( 1 - \sqrt{1 - \frac{s}{r}} \right) \right. \\ & \left. + \frac{rs' - s}{r} \left( 1 - \frac{1}{2\sqrt{1 - (s/r)}} \right) \right\} \\ & \times \left[ \frac{\gamma T_0}{T^2} \left( \frac{T}{qT_0} \right)^{1/2} \left( 1 - \frac{1}{4} \ln \left( \frac{qT_0}{T} \right) \right) \right. \\ & \left. - \frac{\gamma}{qT} \left( \frac{qT_0}{T} \right)^{1/2} \right] \\ & = \frac{Krr_s}{(1 + (r/r_s))^2}. \end{aligned} \quad (30)$$

Keeping the same parameters along with  $q = -0.0000002$  and  $\gamma = 0.9$ , we evaluate shape function numerically and plot versus  $r$  as shown in Figures 4 and 5. The plot of  $s(r)$  versus  $r$  indicates increasing behavior while  $s(r)/r$  meets asymptotically flat condition. The throat of the wormhole is obtained as  $r_0 = 0.008786$  for which first derivative of

shape function holds the corresponding condition; that is,  $s'(0.008786) < 1$ . At throat,  $s(r_0) = r_0$  approximately holds as shown in Figure 4(a).

To check the validity of WEC for this model, inserting (29) in (20)–(22), we obtain

$$\begin{aligned} \rho = & \frac{s'}{r^2} \left[ \frac{\gamma}{2q} \left( \frac{qT_0}{T} \right)^{1/2} \ln \left( \frac{qT_0}{T} \right) - \frac{\gamma T_0}{T} \left( \frac{T}{qT_0} \right)^{1/2} \right] \\ & - \frac{2}{r^2} \left( 1 - \frac{s}{r} - \sqrt{1 - \frac{s}{r}} \right) \\ & \times \left[ -\frac{2s}{r} + 4 \left( 1 - \sqrt{1 - \frac{s}{r}} \right) \right. \\ & \quad \left. + \frac{rs' - s}{r} \left( 1 - \frac{1}{\sqrt{1 - (s/r)}} \right) \right. \\ & \quad \left. + m \left\{ -\frac{2s}{r} + 2 \left( 1 - \sqrt{1 - \frac{s}{r}} \right) \right. \right. \\ & \quad \quad \left. \left. + \frac{rs' - s}{r} \left( 1 - \frac{1}{2\sqrt{1 - (s/r)}} \right) \right\} \right. \\ & \quad \left. \times \left[ \frac{\gamma T_0}{T^2} \left( \frac{T}{qT_0} \right)^{1/2} \left( 1 - \frac{1}{4} \ln \left( \frac{qT_0}{T} \right) \right) \right. \right. \\ & \quad \quad \left. \left. - \frac{\gamma}{qT} \left( \frac{qT_0}{T} \right)^{1/2} \right] \right], \end{aligned} \quad (31)$$

$$\begin{aligned} p_r = & \frac{1}{r^2} \left\{ m \left( 1 - \frac{s}{r} \right) - \frac{s}{r} \right\} \\ & \times \left[ \frac{\gamma}{2q} \left( \frac{qT_0}{T} \right)^{1/2} \ln \left( \frac{qT_0}{T} \right) - \frac{\gamma T_0}{T} \left( \frac{T}{qT_0} \right)^{1/2} \right], \end{aligned} \quad (32)$$

$$\begin{aligned} p_t = & \frac{1}{2r^2} \left[ \frac{\gamma}{2q} \left( \frac{qT_0}{T} \right)^{1/2} \ln \left( \frac{qT_0}{T} \right) - \frac{\gamma T_0}{T} \left( \frac{T}{qT_0} \right)^{1/2} \right] \\ & \times \left[ \frac{m^2}{2} \left( 1 - \frac{s}{r} \right) - \left( 1 + \frac{m}{2} \right) \times \left( s' - \frac{s}{r} \right) \right] \\ & - \frac{1}{r^4} \left( \sqrt{1 - \frac{s}{r}} - \left( 1 + \frac{m}{2} \right) \left( 1 - \frac{s}{r} \right) \right) \\ & \times \left[ -\frac{2s}{r} + 4 \left( 1 - \sqrt{1 - \frac{s}{r}} \right) \right. \\ & \quad \left. + \frac{rs' - s}{r} \left( 1 - \frac{1}{\sqrt{1 - (s/r)}} \right) \right. \\ & \quad \left. + m \left\{ -\frac{2s}{r} + 2 \left( 1 - \sqrt{1 - \frac{s}{r}} \right) \right. \right. \\ & \quad \quad \left. \left. + \frac{rs' - s}{r} \left( 1 - \frac{1}{2\sqrt{1 - (s/r)}} \right) \right\} \right] \end{aligned}$$

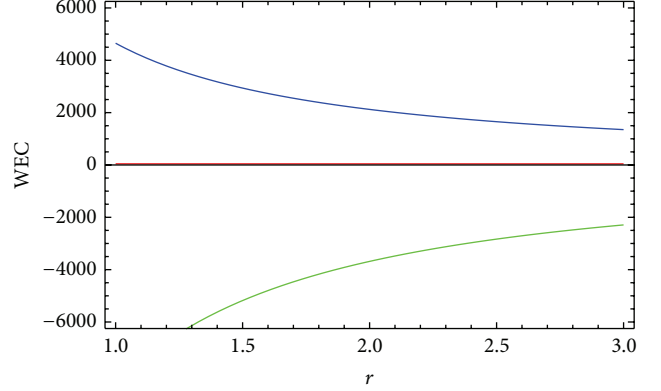


FIGURE 6: Plots of WEC:  $\rho$  versus  $r$  (red curve),  $\rho + p_r$  versus  $r$  (green curve), and  $\rho + p_t$  (blue curve) versus  $r$  for logarithmic model.

$$\begin{aligned} & \times \left\{ \frac{\gamma T_0}{T^2} \left( \frac{T}{qT_0} \right)^{1/2} \times \left( 1 - \frac{1}{4} \ln \left( \frac{qT_0}{T} \right) \right) \right. \\ & \quad \left. - \frac{\gamma}{qT} \left( \frac{qT_0}{T} \right)^{1/2} \right\}]. \end{aligned} \quad (33)$$

Using these expressions, we plot WEC versus  $r$  as shown in Figure 6. The curves corresponding to  $\rho$ ,  $\rho + p_r$  and  $\rho + p_t$  represent the same behavior as for the exponential model. The WEC is violated as the curve of  $\rho + p_r$  indicates negative behavior with respect to  $r$ .

**4.3. Equilibrium Conditions.** Finally, we discuss the equilibrium configuration of the wormhole solutions for both models by taking the generalized Tolman-Oppenheimer-Volkov equation [12, 13]

$$\frac{dp_r}{dr} + \frac{\lambda'}{2} (\rho + p_r) + \frac{2}{r} (p_r - p_t) = 0, \quad (34)$$

for the metric  $ds^2 = \text{diag}(e^{\lambda(r)}, -e^{\nu(r)}, -r^2, -r^2 \sin^2 \theta)$ . Ponce de León suggested this equation for the anisotropic mass distribution in the galactic halo region as follows:

$$-\frac{dp_r}{dr} + \frac{2}{r} (p_t - p_r) - \frac{e^{(\nu-\lambda)/2} M_{\text{eff}}}{r^2} (\rho + p_r) = 0. \quad (35)$$

Here  $M_{\text{eff}} = (1/2)r^2 e^{(\lambda-\nu)/2} \lambda'$  is the effective gravitational mass which is measured from throat to some arbitrary radius  $r$ . This equation indicates the equilibrium configuration for the wormhole solutions by taking gravitational and hydrostatic as well as anisotropic force due to the anisotropic matter distribution. Using (35), these forces are defined, respectively, as

$$\begin{aligned} F_{gf} = & -\frac{\lambda' (\rho + p_r)}{2}, & F_{hf} = & -\frac{dp_r}{dr}, \\ F_{af} = & \frac{2(p_t - p_r)}{r}. \end{aligned} \quad (36)$$

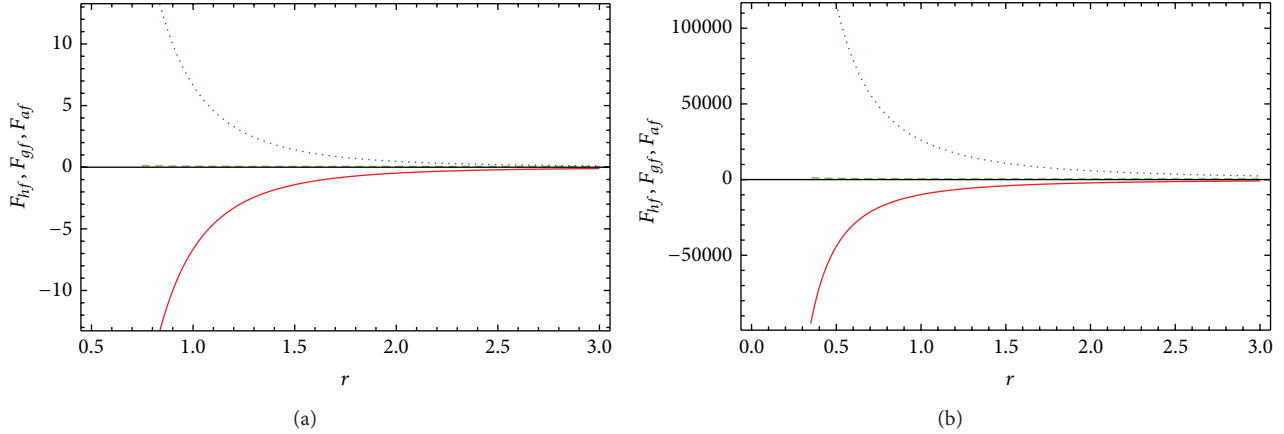


FIGURE 7: Plots of equilibrium conditions for exponential (a) and logarithmic (b)  $f(T)$  models. Red solid curve represents  $F_{hf}$ , green dashed curve represents  $F_{gf}$ , and blue dotted curve represents  $F_{af}$  versus  $r$ .

For the wormhole solutions to be in equilibrium, it is required that

$$F_{gf} + F_{hf} + F_{af} = 0. \quad (37)$$

For exponential and logarithmic models, we use (26)–(28) and (31)–(33), respectively, in (36) along with  $\lambda' = 2g'(r) = m/r$  which represents the derivative of redshift function. The evolution trajectories of the gravitational, hydrostatic, and anisotropy forces are shown in Figure 7 by keeping the same values of constants. These trajectories indicate that combined effect of the forces results in the equilibrium configuration of wormhole solutions for both models. The gravitational force is very small as compared to the hydrostatic and anisotropic forces which represent opposite behavior to each other. This opposite behavior balances the system and stabilizes the wormhole solutions in equilibrium condition.

## 5. Concluding Remarks

The development of wormhole solutions with the help of effective energy-momentum tensor has reawaked interest to study these solutions in modified theories of gravity. We expect some characteristics needed to support traversable wormhole solutions in the galactic halo region. In this paper, we have explored static spherically symmetric wormhole solutions with flat galactic halo curves in  $f(T)$  gravity by taking nondiagonal tetrad and two viable  $f(T)$  models, exponential and logarithmic models. We have explored the wormhole geometry by plotting shape function with its corresponding conditions for both models. The wormhole solutions satisfy all the conditions corresponding to wormhole geometry. We have checked the behavior of WEC for both models and found that WEC is violated for both models by taking some particular values of constants. Finally, we have formulated the equilibrium conditions in order to check the stable configuration. It is worthwhile to mention here that both models represent equilibrium configuration and show compatibility with the results of [12, 13].

Jamil et al. [23] studied wormhole solutions for power-law  $f(T)$  model by taking different equations of state. They assumed constant redshift function while a viable shape function in anisotropic case. The tiny wormhole is found as energy density represents positive behavior for a very small range as  $r < 0.25$ . The NEC is violated for both radial and tangential pressure components and hence no wormhole solution exists in this case except  $r < 0.25$ . For barotropic and isotropic cases, energy conditions hold and wormhole solutions exist but these solutions do not satisfy asymptotically flat condition. In this paper, we have considered flat galactic halo curves in exponential and logarithmic  $f(T)$  models. We have taken a suitable form for the redshift function obtained from flat rotational curve and discussed the wormhole geometry by plotting shape function with its corresponding conditions for both models. The wormhole solutions satisfy all the conditions corresponding to wormhole geometry including asymptotically flat condition. However, energy conditions are violated for both models while equilibrium conditions are satisfied.

## Conflict of Interests

The authors would like to mention here that they have no conflicting interests.

## Acknowledgment


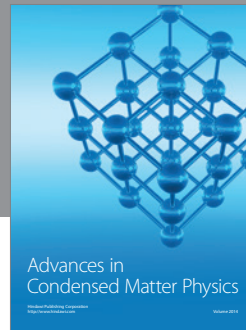
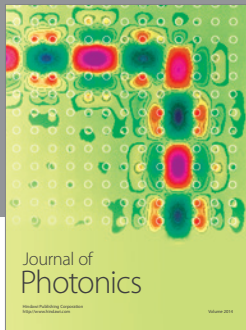
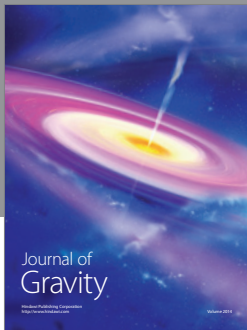
The authors would like to thank the Higher Education Commission, Islamabad, Pakistan, for its financial support through the *Indigenous Ph.D. Fellowship for 5000 Scholars Phase-II, Batch-I*.

## References

- [1] T. Faber and M. Visser, “Combining rotation curves and gravitational lensing: how to measure the equation of state of dark matter in the galactic halo,” *Monthly Notices of the Royal Astronomical Society*, vol. 372, no. 1, pp. 136–142, 2006.



- [2] F. Rahaman, M. Kalam, A. DeBenedictis, A. Usmani, and S. Ray, "Galactic rotation curves and brane-world models," *Monthly Notices of the Royal Astronomical Society*, vol. 389, no. 1, pp. 27–33, 2008.
- [3] K. K. Nandi, A. I. Filippov, F. Rahaman et al., "Features of galactic halo in a brane world model and observational constraints," *Monthly Notices of the Royal Astronomical Society*, vol. 399, no. 4, pp. 2079–2087, 2009.
- [4] E. W. Kolb and M. S. Turner, *The Early Universe*, Addison-Wesley, Reading, Mass, USA, 1990.
- [5] G. Jungman, M. Kamionkowski, and K. Griest, "Supersymmetric dark matter," *Physics Report*, vol. 267, no. 5-6, pp. 195–373, 1996.
- [6] C. G. Böhrer, T. Harko, and F. S. N. Lobo, "Dark matter as a geometric effect in  $f(R)$  gravity," *Astroparticle Physics*, vol. 29, no. 6, pp. 386–392, 2008.
- [7] F. Rahaman, R. Biswas, H. I. Fatima, and N. Islam, "A new proposal for galactic dark matter: effect of  $f(T)$  gravity," *International Journal of Theoretical Physics*, vol. 53, no. 2, pp. 370–379, 2014.
- [8] S. Fay, "Scalar fields properties for flat galactic rotation curves," *Astronomy & Astrophysics*, vol. 41, no. 3, pp. 799–805, 2004.
- [9] K. K. Nandi, I. Valitov, and N. G. Migranov, "Remarks on the spherical scalar field halo in galaxies," *Physical Review D*, vol. 80, no. 4, Article ID 047301, 2009.
- [10] J. F. Navarro, C. S. Frenk, and S. D. M. White, "The structure of cold dark matter halos," *Astrophysical Journal*, vol. 462, p. 563, 1996.
- [11] J. F. Navarro, C. S. Frenk, and S. D. M. White, "A universal density profile from hierarchical clustering," *The Astrophysical Journal*, vol. 490, p. 493, 1997.
- [12] F. Rahaman, P. K. F. Kuhfittig, S. Ray, and N. Islam, "Possible existence of wormholes in the galactic halo region," *European Physical Journal C*, vol. 74, no. 2, pp. 1–7, 2014.
- [13] P. K. F. Kuhfittig, "Gravitational lensing of wormholes in the galactic halo region," *The European Physical Journal C*, vol. 74, article 2818, 2014.
- [14] S.-H. Chen, J. B. Dent, S. Dutta, and E. N. Saridakis, "Cosmological perturbations in  $f(T)$  gravity," *Physical Review D*, vol. 83, Article ID 023508, 2011.
- [15] M. Sharif and S. Rani, "Generalized teleparallel gravity via some scalar field dark energy models," *Astrophysics and Space Science*, vol. 34, no. 1, pp. 217–223, 2013.
- [16] L. Iorio and E. N. Saridakis, "Solar system constraints on  $f(T)$  gravity," *Monthly Notices of the Royal Astronomical Society*, vol. 427, no. 2, pp. 1555–1561, 2012.
- [17] S. Capozziello, P. A. González, E. N. Saridakis, and Y. Vásquez, "Exact charged black-hole solutions in D-dimensional  $f(T)$  gravity: torsion vs curvature analysis," *Journal of High Energy Physics*, vol. 2013, no. 2, article 39, 2013.
- [18] H. M. Sadjadi, "Generalized Noether symmetry in  $f(T)$  gravity," *Physics Letters B*, vol. 718, no. 2, pp. 270–275, 2012.
- [19] M. Farooq, M. Akbar, and M. Jamil, "Dynamics and thermodynamics of (2+1)-dimensional evolving lorentzian wormhole," *AIP Conference Proceedings*, vol. 1295, pp. 176–190, 2010.
- [20] C. G. Böhrer, T. Harko, and F. S. N. Lobo, "Wormhole geometries in modified teleparallel gravity and the energy conditions," *Physical Review D*, vol. 85, Article ID 044033, 2012.
- [21] M. Sharif and S. Rani, "Nonlinear electrodynamics in  $f(T)$  gravity and generalized second law of thermodynamics," *Astrophysics and Space Science*, vol. 34, no. 2, pp. 573–582, 2013.
- [22] M. Sharif and S. Rani, "Thermodynamics in  $f(T)$  gravity and corrected entropies," *The European Physical Journal Plus*, vol. 128, article 96, 2013.
- [23] M. Jamil, D. Momeni, and R. Myrzakulov, "Wormholes in a viable  $f(T)$  gravity," *European Physical Journal C*, vol. 73, no. 1, pp. 1–13, 2013.
- [24] M. Sharif and S. Rani, "Dynamical wormhole solutions in TeX gravity," *General Relativity and Gravitation*, vol. 45, no. 11, pp. 2389–2402, 2013.
- [25] M. Sharif and S. Rani, "Wormhole solutions in  $f(T)$  gravity with noncommutative geometry," *Physical Review D*, vol. 88, Article ID 123501, 2013.
- [26] M. Sharif and S. Rani, "Charged noncommutative wormhole solutions in  $f(T)$  gravity," *The European Physical Journal Plus*, vol. 129, article 237, 2014.
- [27] E. V. Linder, "Einstein's other gravity and the acceleration of the Universe," *Physical Review D*, vol. 81, Article ID 127301, 2010.
- [28] R. Ferraro and F. Fiorini, "Non-trivial frames for  $f(T)$  theories of gravity and beyond," *Physics Letters. B*, vol. 702, no. 1, pp. 75–80, 2011.
- [29] K. Bamba and C. Q. Geng, "Thermodynamics of cosmological horizons in  $f(T)$  gravity," *Journal of Cosmology and Astroparticle Physics*, vol. 2011, article 008, 2011.
- [30] Y.-F. Cai, S.-H. Chen, J. B. Dent, S. Dutta, and E. N. Saridakis, "Matter bounce cosmology with the  $f(T)$  gravity," *Classical and Quantum Gravity*, vol. 28, no. 21, Article ID 215011, 2011.
- [31] K. Karimi and A. Abdolmaleki, "Generalized second law of thermodynamics in  $f(T)$  gravity," *Journal of Cosmology and Astroparticle Physics*, vol. 2012, no. 4, article 007, 2012.
- [32] K. Bamba, C.-Q. Geng, C.-C. Lee, and L.-W. Luo, "Equation of state for dark energy in  $f(T)$  gravity," *Journal of Cosmology and Astroparticle Physics*, vol. 2011, no. 1, article 21, 2011.



**Hindawi**

Submit your manuscripts at  
<http://www.hindawi.com>

